Spatial organization of the ions at the free surface of imidazolium-based ionic liquids

Helga Tóth Ugyonka, György Hantal, István Szilágyi, Nacer Idrissi, Miguel Jorge, Pál Jedlovszky

HAL Id: hal-04676385
https://hal.univ-lille.fr/hal-04676385v1

Submitted on 23 Aug 2024
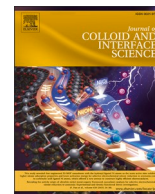
Regular Article

Spatial organization of the ions at the free surface of imidazolium-based ionic liquids

Helga Tóth Ugyonka [a], György Hantal [b], István Szilágyi [c], Abdenacer Idrissi [d], Miguel Jorge [e], Pál Jedlovszky [a],*

[a] Department of Chemistry, Eszterházy Károly Catholic University, Leányka utca 12, H-3300 Eger, Hungary
[b] PULS Group, Department of Physics, Friedrich-Alexander-Universität Erlangen-Nürnberg, Cauerstr. 3, D-91058 Erlangen, Germany
[c] MTA-SZTE Lendület Biocolloids Research Group, Department of Physical Chemistry and Materials Science, Interdisciplinary Excellence Center, University of Szeged, H-6720 Szeged, Hungary
[d] University of Lille, CNRS UMR 8516 -LASIRe - Laboratoire Avancé de Spectroscopie pour les Interactions la Réactivité et l'environnement, 59000 Lille, France
[e] Department of Chemical and Process Engineering, University of Strathclyde, 75 Montrose Street, Glasgow G1 1XJ, United Kingdom

GRAPHICAL ABSTRACT
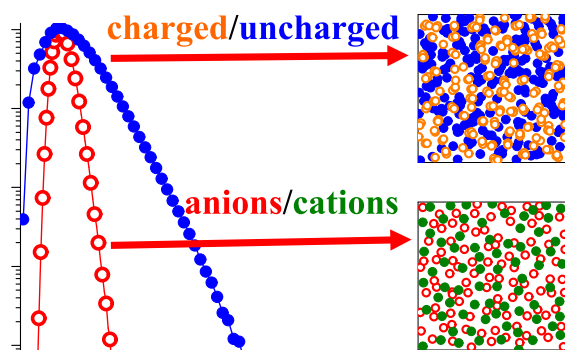
ARTICLE INFO

ABSTRACT

Hypothesis: Experimental information on the molecular scale structure of ionic liquid interfaces is controversial, giving rise to two competing scenarios, namely the double layer-like and "chessboard"-like structures. This issue can be resolved by computer simulation methods, at least for the underlying molecular model. Systematically changing the anion type can elucidate the relative roles of electrostatic interactions, hydrophobic (or, strictly speaking, apolar) effects and steric restrictions on the interfacial properties.

Simulations: Molecular dynamics simulation is combined with intrinsic analysis methods both at the molecular and atomic levels, supplemented by Voronoi analysis of self-association.

Findings: We see no evidence for the existence of a double-layer-type arrangement of the ions, or for their self-association at the surface of the liquid. Instead, our results show that cation chains associate into apolar domains that protrude into the vapour phase, while charged groups form domains that are embedded in this apolar environment at the surface. However, the apolar chains largely obscure the cation groups, to which they are bound, while the smaller and more mobile anions can more easily access the free surface, leading to a somewhat

* Corresponding author.
  E-mail address: jedlovszky.pal@uni-eszterhazy.hu (P. Jedlovszky).

counterintuitive net excess of negative charge at the interface. Importantly, this excess charge could only be identified by applying intrinsic analysis.

1. Introduction

Room temperature ionic liquids (RTILs), i.e., molten salts under ambient conditions, represent a relatively new class of materials. The unusually low melting point of RTILs is a consequence of the chemical structure of the ions constituting them, characterized by low charge density and low symmetry. A large number of RTILs have many attractive properties, such as large thermal stability, broad range of the thermodynamically stable liquid phase, good solvation and miscibility properties, electroconductivity, wide electrochemical window, and tunable physico-chemical properties through the systematic variation of the two ions [1]. These properties enable the use of RTILs in a variety of fields in chemistry and chemical technology [2], such as in separation technology [3], as lubricants [4], or in solar cells [5] and electrochemical devices [6]. RTILs can have co-catalytic effect in homogeneous catalysis, leading to considerable changes in product distribution and stereoselectivity [7]. Certain RTILs can even act as corrosion inhibitors on metallic surfaces [8,9]. Moreover, the extremely low volatility of many RTILs helps to considerably reduce waste and pollution, as compared to the use of conventional volatile organic solvents, making them environmentally friendly, "green" alternatives [10] for chemical synthesis [1], gas capture [11–13], electrochemical reactions [14], heat transfer [15] as well as energy storage and conversion [15]. Further, the inclusion of a paramagnetic species into either of the ions makes the RTIL also being magnetic field responsive, allowing these liquids to be easily separable and recoverable by magnetic separation, and endowing them with additional attractive features, such as luminescence or thermochromic behaviour [16].

This broad range of possible applications generated a great scientific interest in understanding the molecular level properties of RTILs, leading to an explosion of both experimental [17–20] and computational studies [20–30] of such systems in the past decades. These studies led to the general conclusion that the molecular level properties of bulk RTILs and their mixtures with other components are determined by the delicate balance of electrostatic, H-bonding, and hydrophobic interactions acting between various groups of the ions. However, a number of applications of RTILs (e.g., separation, gas capture, electrochemical applications) involve the interface of the ionic liquid with other phases. Although considerably less scientific effort has been devoted to the investigation of the interfacial properties of RTILs than those of their bulk, the interface of RTILs formed with vapour [31] and solid phases [32–36] have also been studied in detail by various experimental means. These studies have been complemented by computer simulation investigations of solid [36–42] and fluid interfaces [43–55] involving various RTILs.

At the molecular scale, fluid interfaces are corrugated by thermal capillary waves, giving rise to a molecular-scale roughness of such surfaces [56]. Therefore, any meaningful analysis of the molecular scale properties of fluid interfaces requires the removal of the smearing effect caused by the neglect of the capillary waves, revealing thus the molecular scale details of the interfacial structure. In other words, it requires the determination of the true, corrugated, so-called "intrinsic" covering surface of the condensed fluid phase(s) in question, formed by the full set of particles that directly contact the opposite phase. The first intrinsic analysis method for liquid surfaces in computer simulations was proposed two decades ago by Chacón and Tarazona in their pioneering work [57], and was rapidly followed by several other, computationally more efficient [58] ones [59–63], some of which are even applicable to surfaces that are not macroscopically flat [62,63]. Intrinsic analysis has since shed new light on various interface-related phenomena, e.g., explanation of the surface tension anomalies of water [64–66],

properties of Newton black films [67], immersion depth of various surfactants [68], kinetic contribution to the surface tension [69], size and charge sign dependence of the surface properties of various ions [70,71], etc. Furthermore, it has been demonstrated that neglecting the effect of capillary wave corrugations causes a large number of particles to be incorrectly classified as both interfacial and non-interfacial [61,72–74]. This misidentification results in a significant systematic error on both structural and dynamical properties of the interface itself [61,70,73,75–77], as well as on the calculated thermodynamic properties of the interfacial system [78].

Unfortunately, the intrinsic surface of RTILs has only scarcely been analyzed in computer simulations [79]; we are certainly aware of only a handful of such studies. In a series of earlier studies, some of us analyzed the intrinsic surface of imidazolium-based RTILs, varying the anions as well as the alkyl chain length of the cations at the RTIL-vapour [47,49], RTIL-liquid [54], and RTIL-gas (i.e., a mixture of CO_2 and N_2) [55] interfaces. Lísal et al. studied the surface of imidazolium-based RTILs containing the bis(trifluoromethylsulfonyl) imide (NTf_2) anion both in the absence [48] and presence [51] of *n*-hexane molecules adsorbing at this surface. These studies revealed unprecedented details of the molecular level properties of the RTIL surface, and led to the general conclusion that, at least for imidazolium-based ionic liquids, the alkyl chains of the cations protrude to the vapour phase, while the imidazolium ring preferentially lies parallel with the interface. Nevertheless, a number of important issues, such as the spatial arrangement of the oppositely charged ions, are still far from being settled [80]. One possibility is that the density decay of the anions upon going away from the liquid surface follows the Goüy-Chapman theory [81] (electric double layer structure). Such arrangement was observed at the surface of muscovite mica [82], and the use of intrinsic surface analysis in computer simulations revealed that the liquid structure at the vicinity of the interface with the vapour phase is often similar to that at solid–liquid interfaces [72]. Electric double layer-like structures at the liquid–vapour interface were indeed observed in simulations of aqueous salt solutions in which the surface affinity of one ion (being a surfactant [83] or just a large and polarizable simple ion, such as I⁻ [84]) is clearly larger than that of the other one [83,84]. Another possibility is that the like ions form separate domains within the surface layer ("chessboard-like" structure) [85]. In addition, the presence of long-range surface forces at interfaces was interpreted in terms of the joint existence of the above-mentioned models [80]. All of these scenarios have been supported by certain experimental findings [86–90], while the importance of the interfacial assembly of ILs in various applications was highlighted [91,92]. Despite these efforts, no consensus view exists yet, and the topic attracts widespread contemporary interest in both fundamental research and more applied disciplines.

In this work, we attempt to answer these questions by carrying out molecular dynamics (MD) simulations of the liquid–vapour interface of four RTILs, consisting of the 1-butyl-3-methylimidazolium (bmim⁺) cation combined with different perfluorinated anions that vary in size, shape, symmetry, and electronic structure: BF_4^-, PF_6^-, NTf_2, and trifluoromethanesulfonate (TfO⁻). To identify the molecularly rugged intrinsic liquid surface as well as the list of particles pertaining both to the surface layer and to subsequent layers beneath the surface, the **i**dentification of the **t**ruly **i**nterfacial **m**olecules (ITIM) method [61] is used. Crucially, we apply ITIM in two distinct ways so as to analyze the composition of each layer in terms of cations and anions (i.e. "molecular view") and also in terms of various atoms and atomic groups (i.e. "atomic view"). We then elucidate the extent and nature of ionic self-association within the surface layer by means of Voronoi analysis [93–95].

2. Methods

2.1. Molecular dynamics simulations

We have carried out MD simulations of the liquid–vapour interfaces of four RTILs, namely [bmim][BF₄], [bmim][PF₆], [bmim][NTf₂], and [bmim][TfO], in the canonical (N,V,T) ensemble at 298 K. Fig. 1 shows the schematic structures of the ions considered in this work. Each simulation box contained 864 ion pairs and was rectangular in shape – i. e., the box length along the X axis, perpendicular to the macroscopic plane of the liquid surface, was always twice as long as that along the Y and Z edges. Table 1 reports the box lengths along the small edges (L) as used in the different simulation systems. To check whether the width of the liquid slab of 60–70 Å is large enough to meaningfully address the possibility of an electric double layer-like ionic arrangement, we have estimated the Debye screening length of the ions, which has turned out to be in the order of a few Angströms, safely smaller than the slab width in every case. Further, to check whether the cross-section of the basic box is large enough to avoid considerable finite size effect error, we have repeated the simulation of [bmim][PF₆] using a basic box with Y and Z edges that are both twice as long as those of the original box. However, no considerable difference between the results obtained in these two basic boxes of different sizes has been observed.

The systems were modelled using the non-polarizable, OPLS-based [96] all-atom force field of Doherty et al. [97], referred to here as the DZGLA model. This force field is reported to reproduce well the experimental density, heat of vaporization, heat capacity, self-diffusion coefficient, viscosity, and interfacial tension of a large number of imidazolium-based RTILs [97]. In particular, the scaling down of the ionic charges with respect to the original OPLS-based model [96] by a factor of 0.8 improved considerably the agreement of the simulated surface tension values with the corresponding experimental data. [97] This agreement is within 1–2 % for [bmim][BF₄] and [bmim][PF₆], while it is still an order of magnitude larger for [bmim][NTf₂] and [bmim][TfO]. However, a 30–40 % deviation of the surface tension from the experimental data is not unusual even for molecular liquids (e.g., most of the widely used water models underestimate the experimental surface tension value by 15–25 % [98]). Further, we are not aware of any RTIL force field that reproduces the surface tension better, in

general, than the DZGLA model. Nevertheless, to assess the dependence of the results on the force field choice, we repeated the [bmim][PF₆] simulations using two earlier force fields: i) the all-atom potential of Bhargava and Balasubramanian (referred to as BB) [99], which is a refinement of the earlier widely used CLaP [100,101] model; and ii) the united atom model of Zhang, Liu and Cao (referred to as ZLC) [102]. All these models use ion charges that are scaled down by a factor of 0.8, since this is known to lead to a better description of both structural and dynamic properties of RTILs. To investigate also the effect of charge scaling, the simulation of [bmim][PF₆] was repeated with the DZGLA model without charge scaling. This unscaled, full-charge version of the DZGLA model [97] is referred to here as DZGLA-FC. The point charges assigned to the different atoms in each model are collected in Tables S1 and S2 of the Supporting Material.

All simulations were performed with the GROMACS MD software, version 2019.3 [103] under standard three-dimensional periodic boundary conditions. The leapfrog algorithm [104] was used to integrate the equations of motion in time steps of 2 fs. All interactions were truncated to zero by applying a spherical cut-off of 13 Å. The long-range contributions of all interactions (i.e. both Lennard-Jones and electrostatics) beyond the cut-off radius were accounted for using the Particle-Mesh-Ewald (PME) approach [105,106] with a Fourier grid spacing of 1.5 Å. In the all-atom simulations, all bond lengths involving hydrogen atoms were constrained to their equilibrium values with the LINCS algorithm [107]. At the start of each simulation, the ions were randomly distributed in a cubic box leading to a loose packing corresponding to roughly 70 % of the expected equilibrium density. The system was then subjected to a steepest descent energy minimization, a 100 ps-long *NVT* simulation, and a 1 ns-long pre-equilibration in the (N,p,T) ensemble with the Berendsen thermostat and barostat [108], in order to obtain a density corresponding to the prescribed ambient temperature and pressure. The simulation box was then extended to twice its equilibrium length along the X axis, thus creating a vacuum phase and, correspondingly, two liquid–vapour interfaces. The extended boxes were subsequently equilibrated for 100 ns in the (N,V,T) ensemble using the v-rescale thermostat [109] with a time constant of 1 ps. Finally, a production run of 100 ns was carried out, during which a sample of 20,000 equilibrium configurations, separated by 5 ps each, was stored for subsequent analysis. To check if the equilibration and production runs
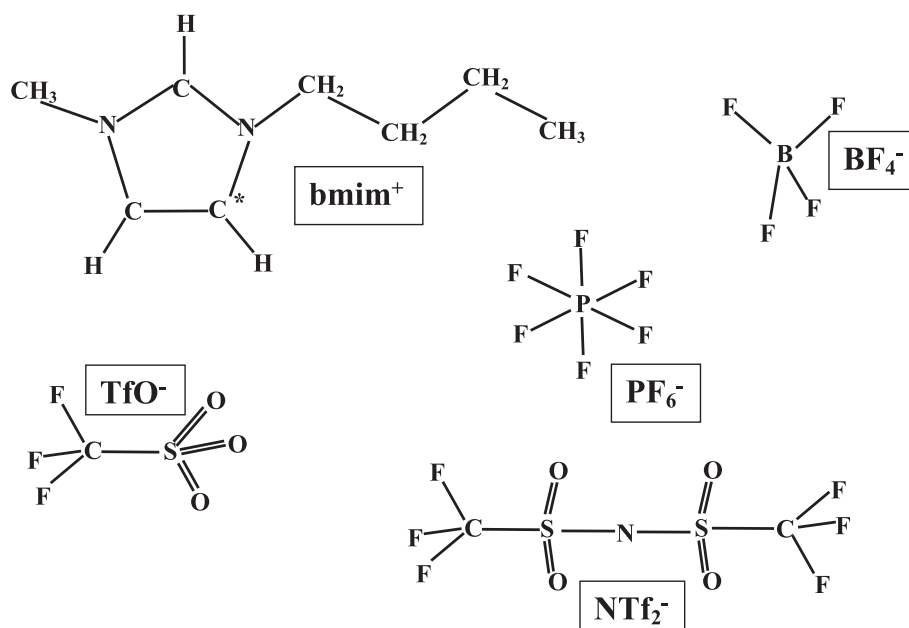

Fig. 1. Schematic structure of the ions considered. The asterisk at the bmim⁺ cation marks the ring C atom that is used as the representative atom in the Voronoi analyses (see the text).

Table 1

Edge length of the basic simulation box in directions parallel to the macroscopic plane of the surface, and number of cations and anions in the first four molecular layers in the different systems simulated.

Anion	Model	L^a/Å	Number of cations				Number of anions			
			layer 1	layer 2	layer 3	layer 4	layer 1	layer 2	layer 3	layer 4
BF_4^-	DZGLA	66.2563	195.4	112.8	157.3	151.8	79.0	205.8	136.3	152.4
PF_6^-	DZGLA	67.2712	184.3	109.0	150.8	144.7	94.2	188.0	130.8	144.2
	DZGLA-FC	67.2712	195.0	104.2	155.7	143.9	88.4	198.6	131.6	147.6
	BB	66.6875	191.0	83.7	146.8	138.7	63.8	200.0	123.3	138.6
	ZLC	66.1753	204.8	92.1	155.3	142.3	91.4	199.8	126.4	147.2
TfO^-	DZGLA	68.0538	198.3	108.7	155.5	145.1	115.5	186.5	126.3	149.2
$NTf2^-$	DZGLA	73.2523	185.9	116.8	148.7	146.1	140.7	167.3	138.5	143.0

[a] The edge length of the basic box along the macroscopic surface normal is $2L$.

were long enough to ensure proper equilibration and sampling, we have performed the analyses of the [bmim][PF$_6$] system, simulated using the DZGLA model, also on the first and last 20 ns long trajectories of the 100 ns long production run. The results agree within statistical noise (see Figure S1 of Supporting Material), confirming that both the equilibration and production stages of the simulations were indeed safely long enough.

2.2. ITIM analysis

The intrinsic surface of each simulated RTIL was identified by the ITIM method [61] which represents, among analogous methods, an excellent balance between computational expense and accuracy [58]. ITIM works by moving a spherical probe from the opposite phase towards the phase of interest along a set of test lines arranged perpendicularly to the macroscopic plane of the surface on a two-dimensional grid. As soon as the probe touches the first particle of the target phase, the latter is tagged as being part of the interfacial layer; the process is then repeated for the next test line. This procedure thus identifies the particles that reside right at the boundary between the two phases, and hence are "seen" from the opposite phase – i.e. the full set of truly interfacial molecules. If the particles that belong to the surface layer are disregarded, the ITIM procedure can be repeated to identify the next subsurface molecular layer, and so on for any desired number of subsequent layers [61]. Furthermore, once the full set of interfacial particles has been identified, a geometric surface passing through those particles can be constructed [72], and the profile of any physical observable can be calculated with respect to this intrinsic, molecularly rugged, capillary wave corrugated surface (i.e. "intrinsic profiles") [74].

Here, we have performed the ITIM analysis in two different ways. First, we identified the subsequent layers beneath the surface in terms of the entire ions. Thus, once the probe has touched any atom of a given ion, the entire ion was identified as belonging to the layer in question. The subsurface layers determined this way are referred to here as "molecular layers". Second, we have identified the different subsurface layers in terms of atoms. For simplicity, the CH, CH$_2$, and CH$_3$ groups of the bmim$^+$ cation were treated as "atoms" here. In this analysis, only the atoms (or CH$_x$ groups) touched by the probe are regarded to be part of the layer in question and, hence, different atoms of the same ion might well belong to different subsurface layers. The layers determined this way are referred to here as "atomic layers".

The ITIM analyses were carried out using the open source and freely available [110] Pytim software [111]. Following earlier recommendations [58,61], the spherical probe radius was set to 2 Å and test lines were arranged on a square grid over the macroscopic plane of the surface, YZ, with a grid spacing of 0.4 Å. It should be emphasized that if the size of the probe sphere is comparable with that of the atoms, the results are rather insensitive to the actual probe radius used [58,61]. Nevertheless, we have repeated the analyses of the [bmim][PF$_6$] system, described by the DZGLA model, using probe radii of 1.75 Å and 2.5 Å, however, the use of a smaller or larger probe has left all of our qualitative conclusions unchanged. To determine the contact distance

between a given atom and the probe sphere, the size of each atom was estimated by its Lennard-Jones distance parameter, σ. The ITIM analysis was performed on the first 4 molecular and 10 atomic layers beneath the liquid surface.

2.3. Voronoi analysis

The Voronoi cell or Voronoi polygon (VP) of a given seed, for a two-dimensional set of seeds, is defined as the locus of points that are closer to this seed than to any other seed in the set [93–95]. Consequently, Voronoi cells cover the plane without overlap or gaps. The area of a Voronoi cell is therefore a measure of the area "belonging" to its central seed, and conversely, its reciprocal quantifies the local density around this seed. It was shown by Zaninetti that if the distribution of the seeds is markedly inhomogeneous, i.e., they form densely packed domains while leaving empty areas between them, the area, A, of the Voronoi cells follows a distribution that exhibits a long, exponentially decaying tail at large areas, while in the case of uniformly distributed seeds, A follows a Gaussian distribution [112]. This provides a way to identify the self-association behaviour of like seeds in a binary system [113] – if the Voronoi analysis is performed considering only one of the components (i.e. disregarding the other one), a homogeneous mixture of the two types of seeds is transformed into a uniform distribution of the seeds considered, resulting still in a Gaussian distribution of A. On the other hand, if the two components form large self-associates, the absence of the disregarded component causes the appearance of large empty areas, and the Voronoi cell area distribution of the analysed component will exhibit the characteristic exponentially decaying tail at large areas [113]. To calculate the area of the Voronoi cells, we have used the algorithm of Ruocco et al. [114] in this study.

3. Results and discussion

The number density profile of the atoms of the cations and anions along the macroscopic surface normal is shown in Fig. 2 for the [bmim][BF$_4$] and [bmim][NTf$_2$] systems, respectively. We have selected these representative systems since they correspond to the two extremes of anion size. The density profiles of the atoms belonging to the first four molecular layers as well as to the first ten atomic layers are also shown.

As it can be seen, the first molecular, and even the first atomic layer, always extends well beyond the X value where the overall density reaches its bulk liquid phase value. Furthermore, the first three and, to a small extent, even the fourth atomic layer contribute to the X range where the overall density falls between the values characteristic of the liquid and vapour phases. This illustrates the importance of using intrinsic analysis to study the structural and dynamical properties of RTIL interfaces, since a non-intrinsic analysis based on, e.g. the Gibbs dividing surface, would introduce a large systematic error into the calculated interfacial properties. In this sense, ionic liquids are not different from simple molecular liquids [72–76,78].

It is also seen that defining the liquid surface in terms of atomic rather than molecular layers corresponds to a considerably higher
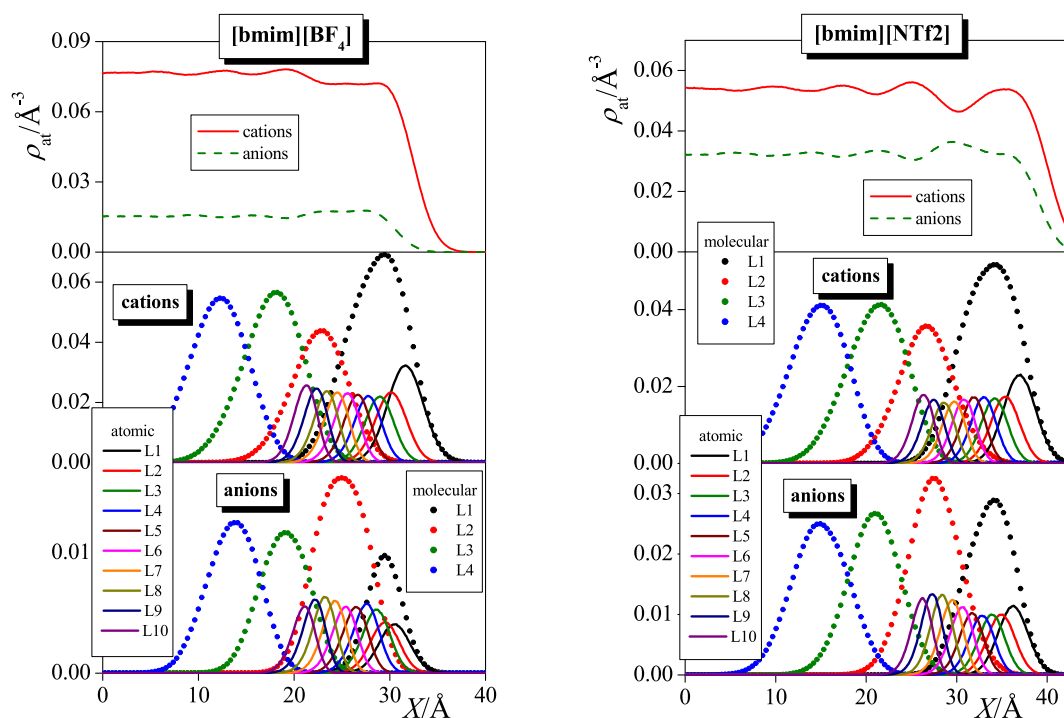
Fig. 2. Atomic number density profile of the cations (red solid lines) and anions (green dashed lines) along the macroscopic surface normal axis, X (top panels), as well as the contributions of the cations (middle panels) and anions (bottom panels) pertaining to the first four molecular layers (symbols) and to the first ten atomic layers (lines) to these profiles, as obtained in [bmim][BF$_4$] (left), and [bmim][NTf$_2$] (right). (For interpretation of the references to colour in this figure legend, the reader is referred to the web version of this article.)

resolution of the interfacial region. Thus, in the case of the smallest ion considered, i.e., BF$_4^-$, the tenth atomic layer extends as deeply into the liquid phase as already the second molecular layer, while in the case of larger ions it does not even reach the inner boundary of the second molecular layer.

3.1. Charge distribution at the liquid surface

The composition of the first four molecular layers of the systems simulated is shown, in terms of cation mole fraction, in Fig. 3. The number of cations and anions pertaining to these layers are collected in Table 1. As it is observed, the first molecular layer consists of considerably more cations than anions, while the second layer is characterized by an excess amount of anions. Thus, the mole fraction of the cations in the first and second layers falls in the range of about 0.6–0.75 and 0.3–0.4, respectively. It is also seen that the actual mole percentage values depend on the type of anion, but they are rather insensitive to the potential model used. Further, from the third molecular layer on, the composition of the subsequent layers rapidly damps to the cation mole fraction of 0.5, i.e., the equimolar composition. These results might suggest that the surface of the ionic liquids is positively charged, and this surface charge is compensated by the excess amount of anions in the second subsurface molecular layer. However, description of the surface properties of these systems in terms of molecular layers corresponds to a rather crude resolution of the surface portion due to the rather large size of the ions. This resolution can be substantially refined by defining the subsequent subsurface layers of the liquid phase in terms of atoms (see Fig. 2).

The mole fraction of the atoms belonging to the anions, as well as to the imidazolium ring (including the H atoms attached to ring C atoms), butyl chain and methyl side group of the cations, are shown in Fig. 4 in all systems simulated. For easier interpretation, the mole fraction values shown are normalized by the overall mole fraction of the given species, $\bar{x}_i$ (i.e. they will tend to 1.0 as the bulk liquid is approached). The surface
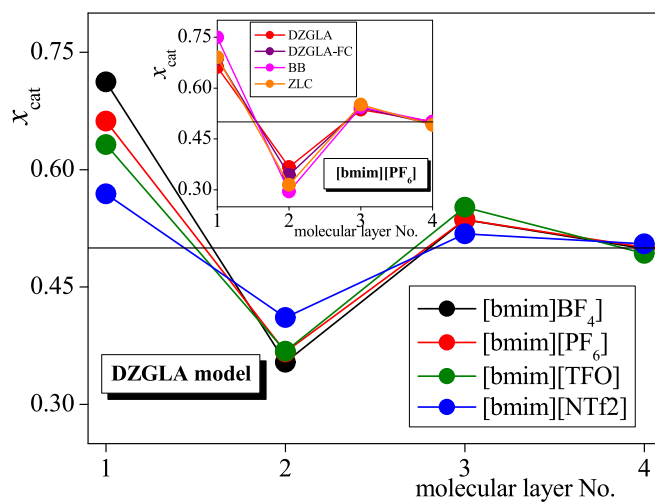

Fig. 3. Mole fraction of the cations in the first four molecular layers of the [bmim][BF$_4$] (black), [bmim][PF$_6$] (red), [bmim][TfO] (green), and [bmim][NTf$_2$] (blue) systems, described by the DZGLA model. The inset shows the same data for [bmim][PF$_6$] as described by the DZGLA (red), DZGLA-FC (purple), BB (magenta), and ZLC (orange) models. Error bars, being in the order or below 0.5% of the mole percentage values, are always smaller than the symbols. The lines connecting the points are just guides to the eye. (For interpretation of the references to colour in this figure legend, the reader is referred to the web version of this article.)

layer is clearly dominated by atoms belonging to the apolar butyl chain, as 60–80 % of the surface atoms belong to these chains in every case. This dominance of the butyl chain atoms vanishes within three atomic layers, as layers 4–5 and 6–8 contain atoms belonging to the imidazolium ring and the methyl side group, respectively, in the largest excess. This observation is in clear agreement with our earlier finding that
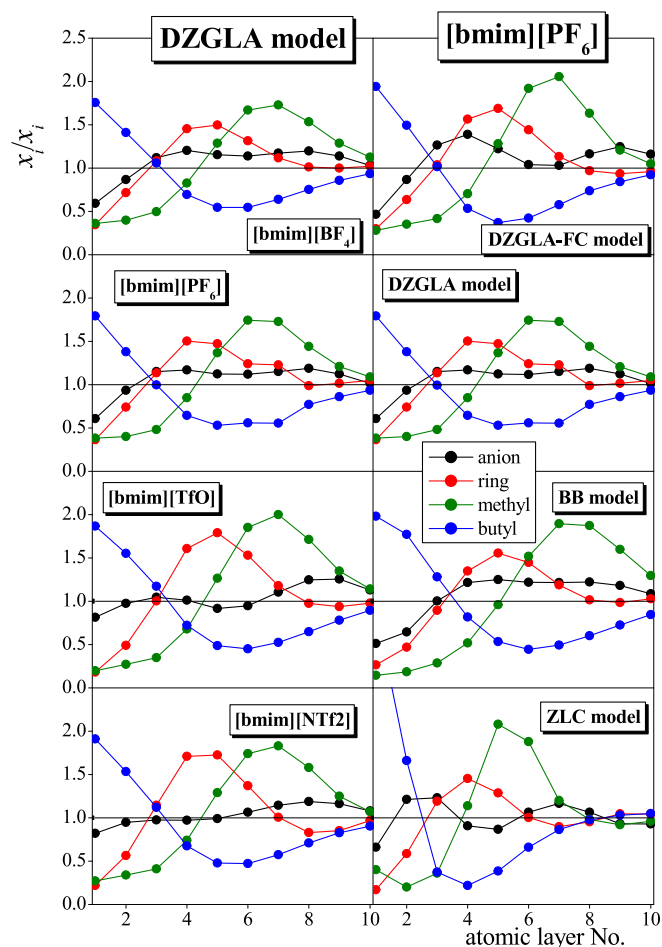
Fig. 4. Mole fraction, x_i, of the atoms belonging to the anions (black), as well as to the imidazolium ring, including H atoms attached to ring C atoms (red), methyl group (green), and butyl chain (blue) of the cations, normalized by their overall mole fraction, $\bar{x}_i$, as obtained in the first ten atomic layers of the different systems simulated with the DZGLA model (left column), and in [bmim][PF$_6$] described with various models (right column). Error bars, being in the order of 0.01, are always smaller than the symbols. The lines connecting the points are just guides to the eye. (For interpretation of the references to colour in this figure legend, the reader is referred to the web version of this article.)

cations preferentially align perpendicularly to the macroscopic plane of the liquid surface, pointing their butyl chain towards the vapour, while the methyl group orients towards the bulk liquid phase. [47,49] Further, atoms of the anions are found to be more or less uniformly distributed along the surface normal axis.

An important observation, however, is that the anions, being considerably smaller than the bmim$^+$ cation, can approach the surface in a larger amount than the positively charged moieties (i.e., the ring and the methyl side group) of the cations (as the black line in Fig. 4 is always above the red and green lines for the first 2–3 atomic layers). Considering that the apolar butyl chain carries no or, in some models, a rather small fractional charge, the above view, inferred from the composition of the subsequent molecular layers in terms of ions, might well be challenged. Namely, the fact that the surface of the liquid is rich in cations can simply be a consequence of the high surface affinity of the apolar butyl groups and, hence, it does not necessarily imply a positively charged surface. In fact, the closer approach of the liquid surface by atoms of the anions than those of the positively charged groups of the cations might well suggest a negatively charged liquid surface.

To clarify this point, we have calculated the charge (surface) density of the subsequent atomic layers, shown in Fig. 5, and also the charge (volume) density profile relative to the capillary wave corrugated
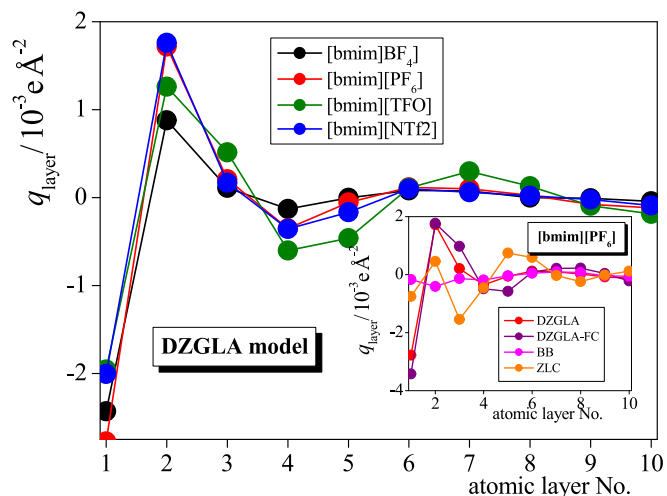

Fig. 5. Excess charge surface density in the first ten atomic layers of the systems simulated using the DZGLA model. The inset shows the same data for [bmim][PF$_6$], described with various models. Colour coding of the systems is the same as in Fig. 3. Error bars, being in the order or below 0.5×10^{-4} e/Å^2, are always smaller than the symbols. The lines connecting the points are just guides to the eye.

intrinsic liquid surface. The obtained intrinsic charge density profiles are plotted in Fig. 6 for the different systems studied here.

As it is observed, the excess charge carried by the first atomic layer is always negative, but it is partly compensated already in the second atomic layer (Fig. 5). Further details of the layer-wise distribution of the excess charge are rather sensitive to the particular model chosen, due to the subtle differences in distributing fractional charges in the different models (see Tables S1 and S2 of Supporting Material), however, interestingly, they are much less sensitive to the type of anion. The only noticeable difference in this respect is that smaller anions induce somewhat higher excess negative charge in the surface atomic layer; a difference that can be well understood considering that smaller anions can be more easily accommodated among the surface butyl chains. On the other hand, the fact that the excess negative charge of the surface is already partly compensated in the second atomic layer – to a large extent, by atoms that are chemically bound to those carrying the negative charge in the surface layer – suggests that the reason for the observed negative surface charge is twofold. Thus, besides the presence of the anions at the liquid surface, the charge distribution within the anions can also contribute to this negative surface charge. Namely, in all the four anions considered, core atoms (i.e., B, P, S and C) carry positive fractional charges, which are overcompensated by the negative fractional charges carried by the outermost (i.e., F and O) atoms (see Table S1 of Supporting Material). This result also implies that the charge separation at the surface of these ionic liquids is very small, and can largely be accounted for by the trivial fact of the charge distribution within the anions.

A deeper insight into the charge distribution at the liquid surface can be obtained through the charge density profile relative to the liquid surface. As it can be seen from Fig. 6, the overall shape of these intrinsic charge density profiles is rather robust. Thus, irrespective of the type of anion and the particular potential model used, the liquid surface always carries some excess negative charge, being, in general, larger for anions of smaller size. However, this negatively charged surface layer is only 5–10 Å wide in all cases. Considering our earlier result concerning the composition of the subsequent atomic layers (Fig. 4), we can conclude that this excess negative surface charge can be attributed to a closer approach by the anions, not being chemically attached to the butyl chains, to the butyl-dominated liquid surface than that of the positively charged moieties of the cations. In other words, the positive groups of
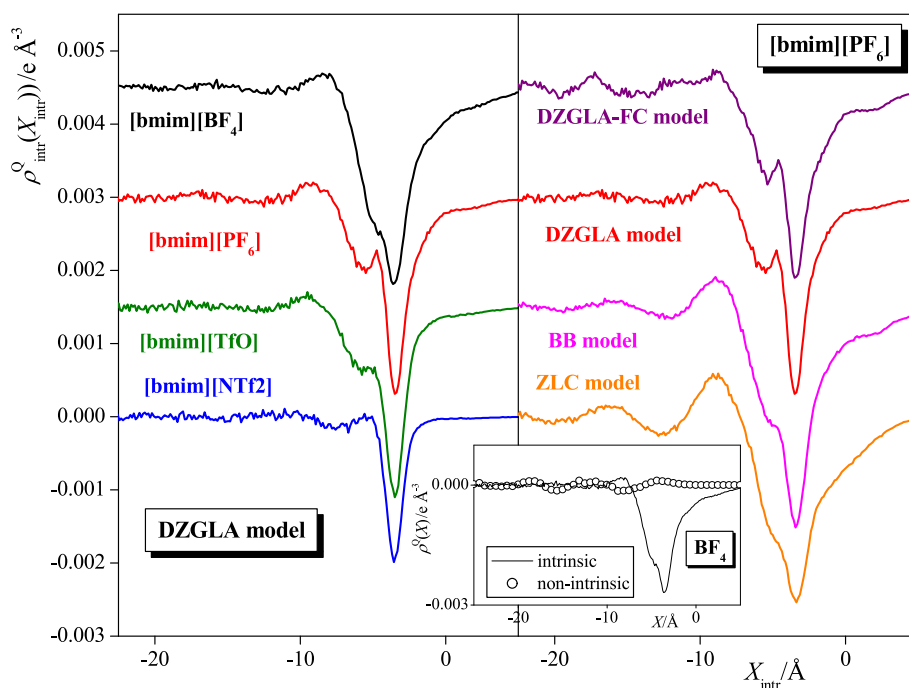
Fig. 6. Intrinsic charge density profile (i.e., relative to the molecularly rough, capillary wave corrugated liquid surface) across the [bmim][BF$_4$] (black), [bmim][PF$_6$] (red), [bmim][TfO] (green), and [bmim][NTf$_2$] systems as described by the DZGLA model (left panel), as well as across the [bmim][PF$_6$] system as described by the DZGLA-FC (purple), DZGLA (red), BB (magenta), and ZLC (orange) models (right panel). The $X_{intr} = 0$ Å value marks the position of the intrinsic liquid surface; negative X_{intr} values correspond to the liquid phase. The curves corresponding to the [bmim][TFO], [bmim][PF$_6$], and [bmim][BF$_4$] systems in the left panel as well as those corresponding to the BB, DZGLA, and DZGLA-FC models (right panel) are shifted up by 0.0015 e/Å^3, 0.003 e/Å^3, and 0.0045 e/Å^3 units, respectively, for clarity. The inset compares the intrinsic and non-intrinsic charge density profiles for [bmim][BF$_4$] (the liquid surface being 0 Å in both cases). (For interpretation of the references to colour in this figure legend, the reader is referred to the web version of this article.)

the cations are "shielded" from the surface by the overwhelming presence of surface-oriented butyl chains attached to them, while the anions are not subject to such steric effects.

Finally, it is worth noting that this excess negative surface charge is indeed a rather small effect in absolute terms, as it can only be detected when considering the intrinsic rather than the average, macroscopically planar liquid surface. In other words, this subtle effect is almost completely blurred by the smearing effect of the capillary waves. This is demonstrated in the inset of Fig. 6, showing the charge density profile in the [bmim][BF$_4$] system both with respect to the capillary wave corrugated intrinsic liquid surface and also to the planar Gibbs dividing surface. Indeed, the non-intrinsic profile is almost completely flat, showing some residual oscillations with an amplitude that is about an order of magnitude smaller than the peak of the intrinsic profile. This finding confirms our earlier claim that the charge separation at the surface of imidazolium-based ionic liquids is very small, and it definitely cannot be understood in terms of an electric double layer. Further, it also demonstrates once again that intrinsic analysis provides a much more detailed picture of the fluid interface than what can be obtained by a conventional, non-intrinsic analysis based on the planar Gibbs-dividing surface.

3.2. Self-association at the liquid surface

As our above findings clearly rule out the presence of a marked electric double layer at the surface of the ionic liquids considered, here we analyze the possible self-association of the like ions and moieties at the surface of these liquids. In analyzing the lateral packing of the entire cations and anions of the surface layer, we have projected a representative, central atom of them onto the macroscopic plane of the surface, YZ. These projections are regarded as a binary system of seeds, on which Voronoi analysis is performed. For the bmim$^+$ cation, we chose the ring C atom bound to the N atom that is attached to the butyl chain (marked

by an asterisk in Fig. 1). For the BF$_4^-$, PF$_6^-$, NTf$_2^-$, and TfO$^-$ anions, the B, P, N, and S atoms, respectively, have been chosen. To investigate the possibility of self-association of like ions within the surface layer, the Voronoi analysis has been done twice for each system: once by disregarding the seeds corresponding to the cations and considering only those of the anions, and once in the other way around.

Fig. 7 shows the VP area distributions obtained in selected systems, together with the Gaussian distributions best fitting to them. To highlight the quality of the fits at high area values, the insets show the distributions along with their fits on a logarithmic scale. As can be seen, the data is reasonably well described by a Gaussian distribution; small deviations from the Gaussian behaviour are only seen at very large areas and low probabilities. This finding indicates that like ions do not form considerable lateral self-associates at the liquid surface; only traces of such behaviour can be observed. Instead, both ions are more or less uniformly distributed along the macroscopic surface plane. This finding is also illustrated in the upper panels of Fig. 8, showing the projections of the surface cations (red) and anions (green) onto the macroscopic plane of the liquid surface, YZ, in an equilibrium configuration of the [bmim][BF4] and [bmim][NTf$_2$] systems, respectively.

In spite of the observed complete lack of association of the like ions, charged and uncharged moieties might well exhibit such a lateral self-association behaviour at the liquid surface, in analogy with their known self-association in the bulk liquid phase [115]. To investigate this possibility, we have divided the heavy (i.e., non-H) atoms of the ions into two groups according to the magnitude of the fractional charge they carry (together with the H atoms attached to them). In this respect, the last three C atoms of the butyl chains are regarded to be 'uncharged', as they carry negligible fractional charges, while all other heavy atoms are regarded as 'charged' ones. Among these 'charged' atoms, only those that occur in the surface atomic layer with non-negligible probability are considered here. These atoms include the F atoms of the anions, the two ring C atoms of the cations that are chemically bound to each other, as
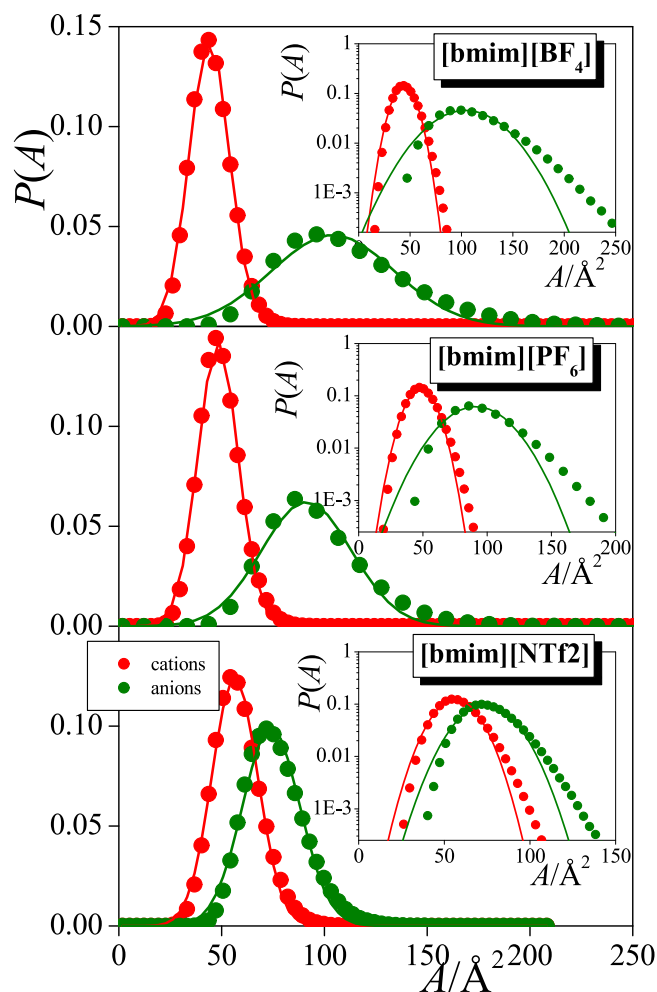
Fig. 7. VP area distribution of the projections of the cations (red symbols) and anions (green symbols), pertaining to the first molecular layer, onto the macroscopic plane of the liquid surface, YZ, as obtained in [bmim][BF$_4$] (top panel), [bmim][PF$_6$] (described by the DZGLA model, middle panel), and [bmim][NTf$_2$] (bottom panel). Each distribution has been calculated by disregarding the other ions in the analysis. Solid curves show the Gaussian functions best fitting the corresponding data. The insets show the same distributions on a logarithmic scale. (For interpretation of the references to colour in this figure legend, the reader is referred to the web version of this article.)

well as the C atom of the methyl side group and first C atom of the butyl chain.

To analyze the possible lateral self-association of the polar and apolar moieties at the liquid surface, we have projected these 'charged' and 'uncharged' atoms, pertaining to the first atomic layer, onto the YZ plane, and performed Voronoi analysis on these projections as described above. The resulting VP area distributions (Fig. 9) corresponding both to the 'uncharged' and 'charged' atoms exhibit a marked, exponentially decaying tail at high areas. This exponential decay, transformed to linear when plotted on a logarithmic scale (see the insets of Fig. 9), clearly cannot be fitted by the Gaussian function. As a consequence, the Gaussian fit of these data are very poor in every case, which is emphasized in the insets of Fig. 9. This behaviour is in clear contrast with what is seen for the entire ions, and reveals that, unlike the entire ions themselves, their uncharged and charged moieties indeed do exhibit marked lateral self-association at the liquid surface. This finding is illustrated in the bottom panels of Fig. 8, showing the projections of the 'charged' (blue) and 'uncharged' (orange) atoms in the YZ plane in equilibrium configurations of the [bmim][BF4] and [bmim][NTf$_2$] systems, respectively. It should finally be noted here that, for the vast

majority of the surface atoms, VP area is below 100 Å^2. Further, similarly to the distributions obtained with molecular resolution (Fig. 7), they never exceed 250 Å^2. Considering that the cross-section of the basic simulation box is in the range of 4.5–5.5 × 10^3 Å^2, i.e., almost two orders of magnitude larger than the typical, and more than one order of magnitude larger than the largest VP area, the obtained results are not expected to be subject of considerable finite size effect error.

The overall picture that emerges from these results is that the interfacial layer is primarily formed of butyl chains that lie perpendicular to the surface [47,49] and self-associate into apolar domains, e.g. forming uncharged "fingers" protruding into the vapour phase. Among these apolar regions, compact charged domains, composed of anions and charged groups of the cations exist. However, the anions, being generally smaller, more mobile [116] and free from attachment to the apolar chains, can more readily approach the surface layer and are hence more "visible" from the opposite phase, mostly at the "troughs" of the corrugated interface. This leads to the observed excess negative surface charge, which is more pronounced for smaller anions. As the bulk liquid is approached, the surface charge profile quickly converges to zero and we see no evidence for a double-layer-type structure.

4. Conclusions

In this paper, we have addressed in detail the long-standing controversy, based on various experimental findings [86–90], concerning the molecular level structure of ionic liquids. These results gave rise to two competing scenarios concerning the spatial arrangement of the ions at such interfaces, namely the electric double layer-like and "chessboard-like" [85] scenarios. Further, the joint existence of these two inter-ionic arrangements has also been considered [80]. Experimental investigations can be well complemented by computer simulations , since the latter yield such a deep, atomistic level insight into the system of interest that cannot be reached by any experimental methods [104]. However, as it is clearly demonstrated here, meaningfully addressing the above issue requires the combination of computer simulation with intrinsic surface analysis [58,61], performed on the atomic rather than molecular level.

In particular, although we have seen a large excess of cations in the surface layer and an excess of anions in the subsequent layer when looking at the surface in the resolution of entire ions (i.e., in terms of 'molecular layers'), the liquid surface has been shown to carry, in fact, a small negative surface charge. This seeming contradiction is resolved considering that the surface is dominated by the uncharged alkyl chains of the cations – hence why there is an overall excess amount of cations at the surface – yet those chains do not contribute to the surface charge. Clearly, the apolar alkyl chains, largely covering the liquid surface, shield the charged parts (i.e., ring and methyl group) of the cations that are chemically bound to them, while they do not have such an effect on the anions. As a consequence, anions can approach the liquid surface in a larger extent than the positively charged groups of the cations, giving thus rise to the observed excess negative surface charge. Further, the excess negative surface charge is only carried by one single atomic layer, indicating that, besides the above effect, this negative surface charge can largely be attributed to the charge distribution within the anions (i.e., the fact that negative fractional charge is carried by the outermost F and O atoms) rather than to the inter-ionic structure. Consistently, the small negative surface charge is seen in the intrinsic profile of the charge density, but it is immediately washed away by the smearing effect of the capillary waves when calculating it relative to the (planar) Gibbs dividing surface rather than to the (corrugated) intrinsic surface. All these results clearly rule out any electric double layer-like scenario at the liquid surface.

Looking at the liquid surface with both a molecular and an atomic resolution has turned out to be useful to assess an alternative hypothesis about the surface structure, i.e., the 'chessboard' scenario. Thus, employing Voronoi analysis [93–95], we have shown that no noticeable
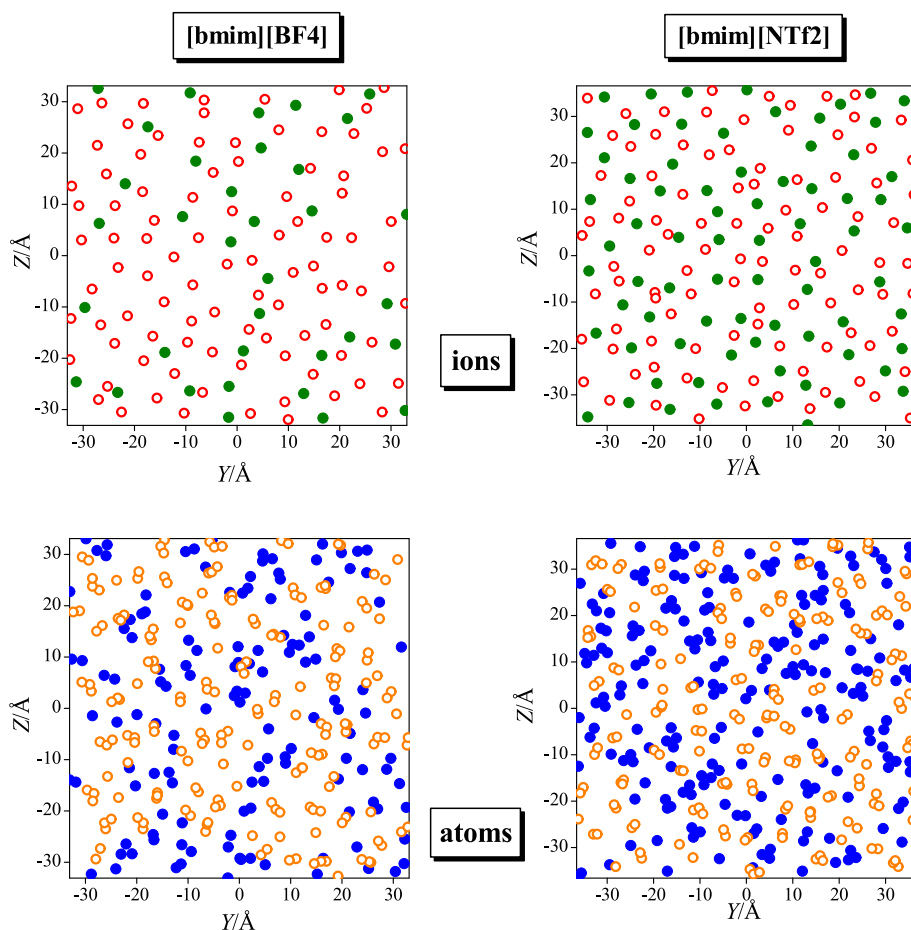
Fig. 8. Instantaneous equilibrium snapshots of the projections of the cations (red open circles) and anions (green filled circles) pertaining to the first molecular layer (top row), as well as of the 'charged' (blue filled circles) and 'uncharged' atoms (orange open circles) pertaining to the first atomic layer (bottom row) of [bmim][BF$_4$] (left column), and [bmim][NTf2] (right column). (For interpretation of the references to colour in this figure legend, the reader is referred to the web version of this article.)

self-association between like ions occurs at the liquid surface. However, similarly to the bulk liquid phase [115], charged and uncharged moieties of the ions indeed form self-associates at the liquid surface, giving rise to a lateral nanostructure formed by such domains. In other words, the 'chessboard' model gives a valid description of the liquid surface, but only if domains of charged and uncharged moieties (and not those of cations and anions) are associated with the black and white tiles of the chessboard. It should also be emphasized that qualitatively similar results have been obtained with four different potential models, including a united atom model and a full-charge model, giving us additional confidence in the above qualitative conclusions. Nevertheless, it should be recognized that the models applied here lack explicit polarization – i. e. they are non-polarizable models. Whether or not this approximation has any effect on the spatial arrangement of the ionic liquid surface should be the subject of future work.

The relevance of our present results in interface science is twofold. First, the inter-ionic organisation at the surface of imidazolium-based ionic liquids is of crucial importance in their applications as lubricants [92], in which the electroresponsive nature of the ionic liquid constituents at the surface is utilized to control friction by changing the electrical potential and expecting the interface to be anion or cation-rich. Besides, a similar argument can be put forward in sensing applications, since the interfacial assembly of ionic liquids directly affects the selectivity and sensitivity of sensors containing ionic liquids as building materials [91]. Second, we have clearly demonstrated the power of combining computer simulation with intrinsic surface analysis, in particular, using atomic scale resolution, in resolving important questions concerning the intermolecular arrangement at fluid surfaces. The relevance of this conceptual advance to the field of interface science can hardly be overestimated, as this methodology can readily be used to elucidate similar issues in a wide variety of fluid surfaces, ranging from interfaces of two immiscible liquids to free surfaces covered by surfactants, and from surfaces of atmospheric droplets to biological interfaces, such as lipid membranes.

CRediT authorship contribution statement

Helga Tóth Ugyonka: Investigation, Formal analysis, Data curation. **György Hantal:** Supervision, Software, Methodology, Data curation. **István Szilágyi:** Conceptualization. **Abdenacer Idrissi:** Supervision, Resources, Conceptualization. **Miguel Jorge:** Writing – review & editing, Validation, Supervision, Formal analysis, Data curation, Conceptualization. **Pál Jedlovszky:** Writing – original draft, Visualization, Supervision, Software, Resources, Project administration, Methodology, Investigation, Funding acquisition, Data curation, Conceptualization.

Declaration of competing interest

The authors declare that they have no known competing financial interests or personal relationships that could have appeared to influence the work reported in this paper.
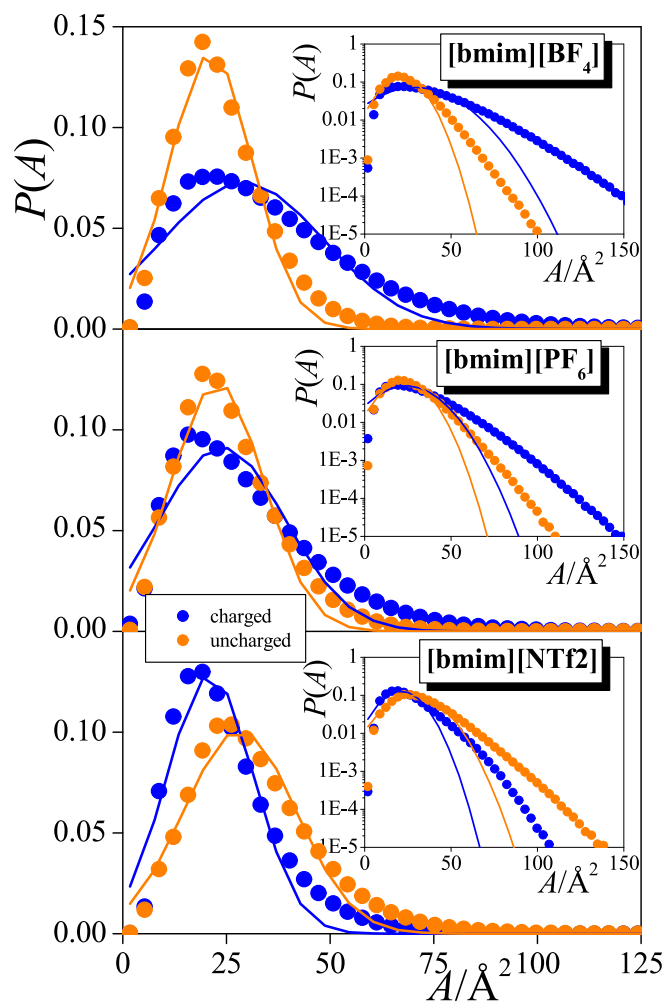
Fig. 9. VP area distribution of the projections of the 'charged' (blue symbols) and 'uncharged' (orange symbols) atoms, pertaining to the first atomic layer, onto the macroscopic plane of the liquid surface, YZ, as obtained in [bmim] [BF$_4$] (top panel), [bmim][PF$_6$] (described by the DZGLA model, middle panel), and [bmim][NTf2] (bottom panel). Each distribution has been calculated by disregarding the other type of atoms in the analysis. Solid curves show the Gaussian functions best fitting the corresponding data. To emphasize the exponential decay of the distributions, the insets show the same distributions on a logarithmic scale. For the definition of the 'charged' and 'uncharged' atoms, see the text. (For interpretation of the references to colour in this figure legend, the reader is referred to the web version of this article.)

Data availability

Data will be made available on request.

Acknowledgements

Appendix A. Supplementary data

Tables showing the fractional charges carried by the individual atoms in the ions considered; a Figure showing comparison of various structural observables as obtained at the beginning and end of the production simulation, and also the numbering of the atoms in the bmim$^+$ cation. Supplementary data to this article can be found online at https://doi.org/10.1016/j.jcis.2024.07.041.

References

[1] P. Wasserscheid, T. Welton (Eds.), Ionic Liquids in Synthesis, Wiley-VCH, Weinheim, 2008.
[2] N.V. Plechkova, K.R. Seddon, Application of ionic liquids in the chemical industry, Chem. Soc. Rev. 37 (2008) 123–150.
[3] H. Watarai, What's happening at the liquid-liquid interface in solvent extraction chemistry? Trends Analyt. Chem. 12 (1993) 313–318.
[4] Y. Zhou, J. Qu, Ionic liquids as lubricant additives: A review, ACS Appl. Mater. Interfaces 9 (2017) 3209–3222.
[5] M. Gratzel, Conversion of sunlight to electric power by nanocrystalline dye sensitized solar cells, J. Photochem. Photobiol. A 164 (2004) 3–14.
[6] P. Hapiot, C. Lagrost, Electrochemical reactivity in room-temperature ionic liquids, Chem. Rev. 108 (2008) 2238–2264.
[7] T. Welton, Room-temperature ionic liquids. solvents for synthesis and catalysis, Chem. Rev. 99 (1999) 2071–2084.
[8] M. Zunita, Y.J. Kelvin, Ionic Liquids as corrosion inhibitor: From research and development to commercialization, Results Eng. 15 (2022) 100562.
[9] N. Kedimar, P. Rao, S.A. Rao, Ionic liquid as an effective green inhibitor for acid corrosion of aluminum composite: Experimental and theoretical considerations, J. Applied Electrochem. 53 (2023) 1473–1489.
[10] R.D. Rogers, K.R. Seddon (Eds.), Ionic Liquids as Green Solvents, Progress and Prospects, American Chemical Society, Washington D.C., 2003.
[11] L.A. Blanchard, D. Hancu, E.J. Beckman, J.F. Brennecke, Green processing using ionic liquids and CO$_2$, Nature 399 (1999) 28–29.
[12] J.L. Anthony, S.N. Aki, E.J. Maginn, J.F. Brennecke, Feasibility of using ionic liquids for carbon dioxide capture, Int. J. Environ. Technol. Manage. 4 (2004) 105–115.
[13] N. Noorani, A. Mehrdad, Solubility of carbon dioxide in some imidazolium and pyridinium-based ionic liquids and correlation with NRTL model, Aus. J. Chem. 75 (2022) 353–361.
[14] J. Avila, C. Corsini, C.M. Correa, M. Rosenthal, A. Pádua, M.C. Costa Gomes, Porous ionic liquids go green, ACS Nano 17 (2023) 19508–19513.
[15] T. Zhou, C. Cui, L. Sun, Y. Hu, H. Lyu, Z. Wang, Z. Song, G. Yu, Energy applications of ionic liquids: Recent developments and future prospects, Chem. Rev. 123 (2023) 12170–12253.
[16] N.M. Figueiredo, I.V. Voroshylova, E.S.C. Ferreira, J.M.C. Marques, M.N.D. S. Cordeiro, Magnetic ionic liquids: Current achievements and future perspectives with a focus on computational approaches, Chem. Rev. 124 (2024) 3392–3415.
[17] V. Overbeck, H. Schröder, A.M. Bonsa, K. Neymeyr, R. Ludwig, Insights into the translational and rotational dynamics of cations and anions in protic ionic liquids by means of NMR fast-field-cycling relaxometry, Phys. Chem. Chem. Phys. 23 (2021) 2663–2675.
[18] B. A. Marekha, V. Koverga, N. Maity, Á. Juhász, F. A. Miannay, A. Inkol, T. Takamuku, P. Jedlovszky, O. N. Kalugin, A. Idrissi, Local structure in mixtures of ionic liquid with molecular solvent: Vibration spectroscopy, NMR and molecular dynamics simulation, in: K. Nishiyama, T. Yamaguchi, T. Takamuku N., Yoshida, (Eds.), Molecular basis of liquids and liquid-based materials, Springer Nature, Singapore, 2021, pp. 289-334, and references therein.
[19] A.E. Khudozhitkov, A.G. Stepanov, D.I. Kolokolov, R. Ludwig, Ion mobility in hydroxy-functionalized ionic liquids depends on cationic clustering: Tracking the alkyl chain length behavior with deuteron NMR relaxation, J. Phys. Chem. B 127 (2023) 9336–9345.
[20] J. Busch, D. Kotwica, L. Al Sheakh, T. Headen, T.G.A. Youngs, D. Paschek, R. Ludwig, Quantification and distribution of three types of hydrogen bonds in mixtures of an ionic liquid with the hydrogen-bond-accepting molecular solvent DMSO explored by neutron diffraction and molecular dynamics simulations, J. Phys. Chem. Lett. 14 (2023) 2684–2691.
[21] B. Kirchner, Ionic liquids from theoretical investigations, in: B. Kirchner (Ed.), Ionic liquids. Topics in current chemistry, Vol. 290, Springer, Berlin, 2010, pp. 213-262.
[22] E.J. Maginn, Molecular Simulation of Ionic Liquids: Current status and future opportunities, J. Phys.: Cond. Matter 21 (2009) 373101.
[23] A. Mondal, S. Balasubramanian, Quantitative prediction of physical properties of imidazolium based room temperature ionic liquids through determination of condensed phase site charges: A refined force field, J. Phys. Chem. B 118 (2014) 3409–3422.
[24] B.A. Marekha, V. Koverga, E. Chesneau, O.N. Kalugin, T. Takamuku, P. Jedlovszky, A. Idrissi, Local structure in terms of nearest-neighbor approach in 1-butyl-3-methylimidazolium-based ionic liquids: MD simulations, J. Phys. Chem. B 120 (2016) 5029–5041.
[25] S. Gehrke, M. von Domaros, R. Clark, O. Hollóczki, M. Brehm, T. Welton, A. Luzar, B. Kirchner, Structure and lifetimes in ionic liquids and their mixtures, Faraday Discuss. 206 (2018) 219–245.
[26] P. Dhakal, J.K. Shah, Recent advances in molecular simulations of ionic liquid-ionic liquid mixtures, Curr. Opin. Green Sustain. Chem. 18 (2019) 90–97.
[27] M.H. Kowsari, S.M. Torabi, Molecular dynamics insights into the nanoscale structural organization and local interaction of aqueous solutions of ionic liquid 1-butyl-3-methylimidazolium nitrate, J. Phys. Chem. B 124 (2020) 6972–6985.
[28] V. Koverga, N. Maity, F.A. Miannay, O.N. Kalugin, Á. Juhász, A. Świątek, K. Polok, T. Takamuku, P. Jedlovszky, A. Idrissi, Voronoi polyhedra as a tool for the characterization of inhomogeneous distribution in 1-butyl-3-methylimidazo-lium cation-based ionic liquids, J. Phys. Chem. B 124 (2020) 10419–10434.
[29] T.M. Chang, S.E. Billeck, Structure, Molecular interactions, and dynamics of aqueous [BMIM][BF$_4$] mixtures: A Molecular Dynamics Study, J. Phys. Chem. B 125 (2021) 1227–1240.

[30] D. Dudariev, V. Koverga, O. Kalugin, F.A. Miannay, K. Polok, T. Takamuku, P. Jedlovszky, A. Idrissi, Insight to the local structure of mixtures of imidazolium-based ionic liquids and molecular solvents from molecular dynamics simulations and Voronoi analysis, J. Phys. Chem. B 127 (2023) 2534–2545.

[31] C.S. Santos, S. Baldelli, Gas-liquid interface of room-temperature ionic liquids, Crit. Rev. 39 (2010) 2136–2145, and references therein.

[32] M. Mezger, H. Schröder, H. Reichert, S. Schramm, J.S. Okasinski, S. Schröder, V. Honkimäki, M. Deutsch, B.M. Ocko, J. Ralston, M. Rohwerder, M. Strattmann, H. Dosch, Molecular layering of fluorinated ionic liquids at a charged sapphire (0001) surface, Science 322 (2008) 424–428.

[33] H. Liu, Y. Liu, J. Li, Ionic liquids in surface electrochemistry, Phys. Chem. Chem. Phys. 12 (2010) 1685–1697.

[34] G. Salas, A. Podgoršek, P.S. Campbell, C.C. Santini, A.A.H. Pádua, M.F. Costa Gomes, K. Philippot, B. Chaudret, M. Turmine, Ruthenium nanoparticles in ionic liquids: Structural and stability effects of polar solutes, Phys. Chem. Chem. Phys. 13 (2011) 13527–13536.

[35] A. Podgoršek, A.S. Pensado, C.C. Santini, M.F. Costa Gomes, A.A.H. Pádua, Interaction energies of ionic liquids with metallic nanoparticles: Solvation and stabilization effects, J. Phys. Chem. C 117 (2013) 3537–3547.

[36] M.V. Fedorov, A.A. Kornyshev, Ionic liquids at electrified interfaces, Chem. Rev. 114 (2014) 2978–3036.

[37] S. Wang, S. Li, Z. Cao, T. Yan, Molecular dynamic simulations of ionic liquids at graphite surface, J. Phys. Chem. C 114 (2010) 990–995.

[38] A.S. Pensado, F. Malberg, M.F. Costa Gomes, A.A.H. Pádua, J. Fernández, B. Kirchner, Interactions and structure of ionic liquids on graphene and carbon nanotubes surfaces, RSC, Adv. 4 (2014) 18017–18024.

[39] H. Weber, T. Bredow, B. Kirchner, Adsorption behavior of the 1,3-dimethylimidazolium thiocyanate and tetracyanoborate ionic liquids at anatase (101) surface, J. Phys. Chem. C 119 (2015) 15137–15149.

[40] H. Weber, M. Salanne, B. Kirchner, Toward an accurate modeling of ionic liquid-TiO$_2$ interfaces, J. Phys. Chem. C 119 (2015) 25260–25267.

[41] I.V. Voroshylova, H. Ers, V. Koverga, B. Docampo- Álvarez, P. Pikma, V. B. Ivaništšev, M.N.D.S. Cordeiro, Ionic liquid–metal interface: The origins of capacitance peaks, Electrochim. Acta 379 (2021) 138148.

[42] M.J. Voegtle, T. Pal, A.K. Pennathur, J.G. Patrow, S. Sarkar, Q. Cui, J.M. Dawlaty, Interfacial polarization and ionic structure at the ionic liquid–metal interface studied by vibrational spectroscopy and molecular dynamics simulations, J. Phys. Chem. B 125 (2021) 2741–2753.

[43] G. Chevrot, R. Schurhammer, G. Wipff, Molecular dynamics simulation of the aqueous interface with the [BMI][PF$_6$] ionic liquid: Comparison of different solvent models, Phys. Chem. Chem. Phys. 8 (2006) 4166–4174.

[44] B.L. Bhargava, S. Balasubramanian, Layering at an ionic liquid−vapor interface: A molecular dynamics simulation study of [bmim][PF6], J. Am. Chem. Soc. 128 (2006) 10073–10078.

[45] R.M. Lynden-Bell, M. Del Pópolo, Simulation of the surface structure of butylmethylimidazolium ionic liquids, Phys. Chem. Chem. Phys. 8 (2006) 949–954.

[46] S.S. Sarangi, S.G. Raju, S. Balasubramanian, Molecular dynamics simulations of ionic liquid–vapour interfaces: Effect of cation symmetry on structure at the interface, Phys. Chem. Chem. Phys. 13 (2011) 2714–2722.

[47] G. Hantal, M.N.D.S. Cordeiro, M. Jorge, What does an ionic liquid surface really look like? Unprecedented details from molecular simulations, Phys. Chem. Chem. Phys. 13 (2011) 21230–21232.

[48] M. Lísal, Z. Posel, P. Izák, Air–liquid interfaces of imidazolium-based [TF$_2$N⁻] ionic liquids: insight from molecular dynamics simulations, Phys. Chem. Chem. Phys. 14 (2012) 5164–5177.

[49] G. Hantal, I. Voroshylova, M.N.D.S. Cordeiro, M. Jorge, A systematic molecular simulation study of ionic liquid surfaces using intrinsic analysis methods, Phys. Chem. Chem. Phys. 14 (2012) 5200–5213.

[50] X. Paredes, J. Fernández, A.A.H. Pádua, P. Malfreyt, F. Malberg, B. Kirchner, A. S. Pensado, Using molecular simulation to understand the structure of [C$_2$C$_1$im]⁺–alkylsulfate ionic liquids: Bulk and liquid–vapour interfaces, J. Phys. Chem. B 116 (2012) 14159–14170.

[51] M. Lísal, P. Izák, Molecular dynamics simulations of n-hexane at 1-butyl-3-methylimidazolium bis(trifluoromethylsulfonyl) imide interface, J. Chem. Phys. 139 (2013) 014704.

[52] X. Paredes, J. Fernández, A.A.H. Pádua, P. Malfreyt, F. Malberg, B. Kirchner, A. S. Pensado, Bulk and liquid-vapour interface of pyrrolidinum-based ionic liquids: A molecular simulation study, J. Phys. Chem. B 118 (2014) 731–742.

[53] F. Malberg, O. Hollóczki, M. Thomas, B. Kirchner, En route formation of ion pairs at the ionis liquid-vacuum interface, Struct. Chem 26 (2015) 1343–1349.

[54] G. Hantal, M. Sega, S. Kantorovich, C. Schröder, M. Jorge, Intrinsic structure of the interface of partially miscible fluids: an application to ionic liquids, J. Phys. Chem. C 119 (2015) 28448–28461.

[55] D.N. Lapshin, M. Jorge, E.E.B. Campbell, L. Sarkisov, On competitive gas adsorption and absorption phenomena in thin films of ionic liquids, J. Mater. Chem. A 8 (2020) 11781–11799.

[56] J.S. Rowlinson, B. Widom, Molecular theory of capillarity, Dover Publications, Mineola, 2002.

[57] E. Chacón, P. Tarazona, P Intrinsic profiles beyond the capillary wave theory: A Monte Carlo study, Phys Rev. Letters 91 (2003) 166103.

[58] M. Jorge, P. Jedlovszky, M.N.D.S. Cordeiro, A critical assessment of methods for the intrinsic analysis of liquid interfaces. 1. Surface site distributions, J. Phys. Chem. C. 114 (2010) 11169–11179.

[59] J. Chowdhary, B.M. Ladanyi, Water-Hydrocarbon Interfaces: Effect of hydrocarbon branching on interfacial structure, J. Phys. Chem. b 110 (2006) 15442–15453.

[60] M. Jorge, M.N.D.S. Cordeiro, Intrinsic structure and dynamics of the water/nitrobenzene interface, J. Phys. Chem. c 111 (2007) 17612–17626.

[61] L.B. Pártay, G. Hantal, P. Jedlovszky, Á. Vincze, G. Horvai, A new method for determining the interfacial molecules and characterizing the surface roughness in computer simulations. Application to the liquid–vapor interface of water, J. Comp. Chem. 29 (2008) 945–956.

[62] A.P. Willard, D. Chandler, Instantaneous liquid interfaces, J. Phys. Chem. b 114 (2010) 1954–1958.

[63] M. Sega, S. Kantorovich, P. Jedlovszky, M. Jorge, The generalized identification of truly interfacial molecules (ITIM) algorithm for nonplanar interfaces, J. Chem. Phys. 138 (2013) 044110.

[64] M. Sega, G. Horvai, P. Jedlovszky, Microscopic origin of the surface tension anomaly of water, Langmuir 30 (2014) 2969–2972.

[65] M. Sega, G. Horvai, P. Jedlovszky, Two-dimensional percolation at the free water surface and its relation with the surface tension anomaly of water, J. Chem. Phys. 141 (2014) 054707.

[66] A. Gorfer, C. Dellago, M. Sega, High-Density Liquid (HDL) adsorption at the supercooled water/vapour interface and its possible relation to the second surface tension inflection point, J. Chem. Phys. 158 (2023) 054503.

[67] F. Bresme, E. Chacón, H. Martínez, P. Tarazona, Adhesive transitions in Newton black films: A computer simulation study, J. Chem. Phys. 134 (2011) 214701-1–214712.

[68] N. Abrankó-Rideg, M. Darvas, G. Horvai, P. Jedlovszky, Immersion depth of surfactants at the free water surface: A computer simulation and ITIM analysis study, J. Phys. Chem. B 117 (2013) 8733–8746.

[69] M. Sega, B. Fábián, P. Jedlovszky, Nonzero ideal gas contribution to the surface tension of water, J. Phys. Chem. Letters 8 (2012) 2608–2612.

[70] G. Hantal, R.A. Horváth, J. Kolafa, M. Sega, P. Jedlovszky, Surface affinity of alkali and halide ions in their aqueous solution: Insight from intrinsic density analysis, J. Phys. Chem. B 124 (2020) 9884–9897.

[71] G. Hantal, M. Klíma, L. McFegan, J. Kolafa, P. Jedlovszky, Does the sign of charge affect the surface affinity of simple ions? J. Phys. Chem. B 127 (2023) 6205–6216.

[72] M. Jorge, G.y. Hantal, P. Jedlovszky, M.N.D.S. Cordeiro, A critical assessment of methods for the intrinsic analysis of liquid interfaces. 2. Density profiles, J. Phys. Chem. c. 114 (2010) 18656–18663.

[73] G. Hantal, M. Darvas, L.B. Pártay, G. Horvai, P. Jedlovszky, Molecular level properties of the free water surface and different organic liquid/water interfaces, as seen from ITIM analysis of computer simulation results, J. Phys.: Condens. 22 (Matter 2010,) 284112.

[74] M. Sega, B. Fábián, P. Jedlovszky, Layer-by-layer and intrinsic analysis of molecular and thermodynamic properties across soft interfaces, J. Chem. Phys. 143 (2015) 114709.

[75] L.B. Pártay, P. Jedlovszky, Á. Vincze, G. Horvai, Properties of Free Surface of Water-Methanol Mixtures. Analysis of the truly interfacial molecular layer in computer simulation, J. Phys. Chem. b. 112 (2008) 5428–5438.

[76] B. Fábián, G. Horvai, M. Sega, P. Jedlovszky, Single particle dynamics at the intrinsic surface of various apolar, aprotic dipolar, and hydrogen bonding liquids as seen from computer simulations, J. Phys. Chem. b. 121 (2017) 5582–5594.

[77] P. Malgaretti, U. Bafile, R. Vallauri, P. Jedlovszky, M. Sega, Surface viscosity in simple liquids, J. Chem. Phys. 158 (2023) 114705.

[78] L.B. Pártay, G. Horvai, P. Jedlovszky, Temperature and pressure dependence of the properties of the liquid-liquid interface. A computer simulation and identification of the truly interfacial molecules investigation of the water-benzene system, J. Phys. Chem. c. 114 (2010) 21681–21693.

[79] M. Lbadaoui-Darvas, A. Idrissi, P. Jedlovszky, Computer simulation of the surface of aqueous ionic and surfactant solutions, J. Phys. Chem. B 126 (2022) 751–765.

[80] M.A. Gebbie, A.M. Smith, H.A. Dobbs, A.A. Lee, G.G. Warr, X. Banquy, M. Valtiner, M.W. Rutland, J.N. Israelachvili, S. Perkin, R. Atkin, Long range electrostatic forces in ionic liquids, Chem. Commun. 53 (2017) 1214–1224.

[81] R.J. Hunter, Foundations of Colloid Science, Vol. I, Oxford University Press, Oxford, 1989.

[82] M.A. Gebbie, M. Valtiner, X. Banquy, E.T. Fox, W.A. Henderson, J.N. Israelachvili, Ionic liquids behave as dilute electrolyte solutions, Proc. Natl. Acad. Sci. USA 110 (2013) 9674–9679.

[83] G.y. Hantal, L.B. Pártay, I. Varga, P. Jedlovszky, T. Gilányi, Counterion and surface density dependence of the adsorption layer of ionic surfactants at the vapour-aqueous solution interface: A computer simulation study, J. Phys. Chem. B 111 (2007) 1769–1774.

[84] G.y. Hantal, J. Kolafa, M. Sega, P. Jedlovszky, Polarization effects at the surface of aqueous alkali halide solutions, J. Mol. Liquids 385 (2023) 122333.

[85] J.A. Smith, O. Werzer, G.B. Webber, G.G. Warr, R. Atkin, Surprising particle stability and rapid sedimentation rates in an ionic liquid, J. Phys. Chem. Lett. 1 (2010) 64–68.

[86] J.C. Riedl, M.A. Akhavan Kazemi, F. Cousin, E. Dubois, S. Fantini, S. Lois, R. Perzynski, V. Peyre, Colloidal dispersions of oxide nanoparticles in ionic liquids: elucidating the key parameters, Nanoscale Adv. 2 (2020) 1560–1572.

[87] X.W. Mao, P. Brown, C. Cervinka, G. Hazell, H. Li, Y.Y. Ren, D. Chen, R. Atkin, J. Eastoe, I. Grillo, A.A.H. Pádua, M.F. Costa Gomes, T.A. Hatton, Self-assembled nanostructures in ionic liquids facilitate charge storage at electrified interfaces, Nat. Mater. 18 (2019) 1350–1357.

[88] J. Wang, J.J. Buzolic, J.W. Mullen, P.A. Fitzgerald, Z.M. Aman, M. Forsyth, H. Li, D.S. Silvester, G.G. Warr, R. Atkin, Nanostructure of locally concentrated ionic

liquids in the bulk and at graphite and gold electrodes, ACS Nano 17 (2023) 21567–21584.

[89] D. Takács, M. Tomšič, I. Szilagyi, Effect of water and salt on the colloidal stability of latex particles in ionic liquid solutions, Colloid Interfac. 6 (2022) 2.

[90] Q.L. Zheng, Z.A.H. Goodwin, V. Gopalakrishnan, A.G. Hoane, M.W. Han, R. X. Zhang, N. Hawthorne, J.D. Batteas, A.A. Gewirth, R.M. Espinosa-Marzal, Water in the electrical double layer of ionic liquids on graphene, ACS Nano 17 (2023) 9347–9360.

[91] D.S. Silvester, R. Jamil, S. Doblinger, Y.X. Zhang, R. Atkin, H. Li, Electrical double layer structure in ionic liquids and its importance for supercapacitor, battery, sensing, and lubrication applications, J. Phys. Chem. C 125 (2021) 13707–13720.

[92] M. Radiom, Ionic liquid-solid interface and applications in lubrication and energy storage, Curr. Opin. Colloid Interface Sci. 39 (2019) 148–161.

[93] G.F. Voronoi, Recherches sur le paralléloèders primitives, J. Reine Angew. Math. 134 (1908) 198–287.

[94] A. Okabe, B. Boots, K. Sugihara, S.N. Chiu, Spatial tessellations: Concepts and applications of Voronoi diagrams, John Wiley, Chichester, 2000.

[95] N.N. Medvedev, The Voronoi-Delaunay method in the structural investigation of non-crystalline systems, SB RAS, Novosibirsk, 2000 in Russian.

[96] S.V. Sambasivarao, O. Acevedo, Development of OPLS-AA force field parameters for 68 unique ionic liquids, J. Chem. Theory Comput. 5 (2009) 1038–1050.

[97] B. Doherty, X. Zhong, S. Gathiaka, B. Li, O. Acevedo, Revisiting OPLS force field parameters for ionic liquid simulations, J. Chem. Theory Comput. 13 (2017) 6131–6145.

[98] C. Vega, J.L.F. Abascal, Simulating water with rigid non-polarizable models: a general perspective, Phys. Chem. Chem. Phys. 13 (2011) 19663–19668.

[99] B.L. Bhargava, S. Balasubramanian, Refined potential model for atomistic simulations of ionic liquid [bmim][PF$_6$], J. Chem. Phys. 127 (2007) 114510.

[100] J.N. Canongia Lopes, J. Deschamps, A.A.H. Pádua, Modeling ionic liquids using a systematic all-atom force field, J. Phys. Chem. B 108 (2004) 2038–2047.

[101] J.N. Canongia Lopes, J. Deschamps, A.A.H. Pádua, Modeling ionic liquids using a systematic all-atom force field (addition and correction), J. Phys. Chem. B 108 (2004) 11250.

[102] X. Zhong, Z. Liu, D. Cao, Improved classical united-atom force field for imidazolium-based ionic liquids: Tetrafluoroborate, hexafluorophosphate,

methylsulfate, trifluoromethylsulfonate, acetate, trifluoroacetate, and bis (trifluoromethylsulfonyl) amide, J. Phys. Chem. B 115 (2011) 10027–10040.

[103] M.J. Abraham, T. Murtola, R. Schulz, S. Páll, J.C. Smith, B. Hess, E. Lindahl, GROMACS: High performance molecular simulations through multi-level parallelism from laptops to supercomputers, SoftwareX 1–2 (2015) 19–25.

[104] M.P. Allen, D.J. Tildesley, Computer simulation of liquids, Clarendon Press, Oxford, 1987.

[105] U. Essman, L. Perera, M.L. Berkowitz, T. Darden, H. Lee, L.G. Pedersen, A smooth particle mesh Ewald method, J. Chem. Phys. 103 (1995) 8577–8594.

[106] P.J. in't Veld, A.E. Ismail, G.S. Grest, Application of Ewald Summations to long–range dispersion forces, J. Chem. Phys. 127 (2007) 144711.

[107] B. Hess, P-LINCS: A parallel linear constraint solver for molecular simulation, J. Chem. Theory Comput. 4 (2008) 116–122.

[108] H.J.C. Berendsen, J.P.M. Postma, A. DiNola, J.R. Haak, Molecular dynamics with coupling to an external bath, J. Chem. Phys. 81 (1984) 3684–3691.

[109] G. Bussi, D. Donadio, M. Parrinello, Canonical sampling through velocity rescaling, J. Chem. Phys. 126 (2007) 014101.

[110] URL: https://github.com/Marcello-Sega/pytim (last accessed: 07 April 2024).

[111] M. Sega, G. Hantal, B. Fábián, P. Jedlovszky, Pytim: A python package for the interfacial analysis of molecular simulations, J. Comp. Chem. 39 (2018) 2118–2125.

[112] L. Zaninetti, The Voronoi Tessellation generated from different distributions of seeds, Phys. Letters A 165 (1992) 143–147.

[113] A. Idrissi, P. Damay, K. Yukichi, P. Jedlovszky, Self-association of urea in aqueous solutions: A Voronoi polyhedron analysis study, J. Chem. Phys. 129 (2008) 164512.

[114] G. Ruocco, M. Sampoli, R. Vallauri, Analysis of the network topology in liquid water and hydrogen sulphide by computer simulation, J. Chem. Phys. 96 (1992) 6167–6176.

[115] J.N. Canongia Lopes, A.A.H. Pádua, Nanostructural organization in ionic liquids, J. Phys. Chem. B 110 (2006) 3330–3335.

[116] H. Tóth Ugyonka, Gy. Hantal, I Szilágyi, A. Idrissi, M. Jorge, P. Jedlovszky, unpublished results.